

# Full-Wave Modeling of Grounding System: Evaluation The Effects of Multi-Layer Soil and Length of Electrode on Ground Potential Rise

M. Ghomi, H.R. Mohammadi, H. R. Karami, C. L. Bak, F. F. da Silva, H. Khazraj

**Abstract**—The accurate modelling of grounding system is important part of power system transient studies. It is special significance for high frequency phenomena like lightning striking one tower of power transmission lines, when the length of electrodes and soil layers can effect accuracy of grounding system modeling. This paper presents the effects of electrode length and multilayer soil in the ground potential rise using impressed-current model as the excitation. The input impedance for different lengths of vertical electrode in wide-band frequency is obtained by making use of the method of moments solution to Maxwell's equations. The subsequent stroke has high frequency contents and the dynamic behavior of grounding system must be taken into account. Therefore, the input impedance is used for ground potential rise calculations. input impedance depends on the parameters of both layers and the length of electrode. Additionally, different soil resistivity, different electrode lengths in uniform and multilayer soil are simulated. The simulation results in this paper show that the geometry and accurate model for grounding system are important in ground potential rise.

**Keywords**—Grounding system, ground potential rise, input impedance, multi-layer soil.

## I. INTRODUCTION

Proper grounding systems (GS) design play a key role in high-voltage overhead transmission lines operation [1]. Back-flashover is one of the main causes of insulator strings breakdown. It occurs as a result of direct lightning stroke to the tower body or shield wires and injects impulse current with high amplitude and very high steepness to the phase conductors, injection of these impulse currents generate voltages with high amplitude and very high steepness, which in turn cause phase to ground faults and insulator string damaging. Inadequate GS can make the operators and customers incur extra cost due to the increase in maintenance services, the need to replacement of damaged insulators and the cut of electricity due to line outages [2], [3]. A wide-band modeling of grounding system up to a few MHz is necessary for a proper estimation of the overvoltage also owing to the high frequency contents of lightning current. The model should be well suited to be applied in EMTP tools which are normally

used for the transient analysis in time-domain. At the same time, GS detailed modeling is a challenging task because of the complex nature of the soil such as multilayered soil, frequency dependence electrical parameters, nonlinearity and ionization [4], [5]. Different modeling methods for GS have been proposed in the past few years [6], [7]. Nevertheless, they cannot guarantee accurate modeling able to deal with a multilayer soil and others complex phenomena such as soil frequency dependence. The full-wave electromagnetic field methods applied for the studies of GSs are based on both the time and frequency domain numerical solution of Maxwell's equations. The finite element method (FEM) used in [8], the method of moments (MoM) used in [9], the transmission line modeling (TLM) Methods applied in [10] and finite difference time domain (FDTD) method used in [11] are example of multiple significant methods. Nevertheless, the MoM is applied in most of the studies in recent years because of computation time and simply in implementation. Soil is represented as linear, homogeneous and multilayer, which is identified by a resistivity, permittivity, and permeability. Though it is well recognized that the soil presents complex phenomena [12]. However, no comprehensive precise study has been given yet for calculationg the GPR of GS with multilayer soil structure. This paper applies the full-wave approach for subsequent impulse current based on MoM [13], [14], [15]. This numerical method is considered as the most accurate since it is based on least neglects in comparison to the methods based on transmission line and circuit theory. In this paper, a technique for input impedance calculation of GSs used in [16], [17] is used, which is very useful in the transient analysis because it depends solely on geometry parameters like electromagnetic characteristic of the ground electrodes and length [12]. The proposed method applied in two stages. First, the input impedance of the GS is calculated from DC to several MHz. The GS is acknowledged as a single-port electromagnetic system where the input impedance is estimated by obtaining use of the MoM solution. Then, the obtained input impedance is used for ground potential rise (GPR) calculation for insulation coordination studies.

The paper is arranged as follows. Section II briefly explains the theory and the formulations of GS buried in multilayer soil. The section III, numerical results of input impedance with a different length of electrode and soil resistivity is analyzed. The effects assessment of a multi-layer soil and length of the electrode on GPR is briefly explained in section IV. Finally, the conclusion of work is presented in section V.

---

M. Ghomi, C. L. Bak, F. F. da Silva, H. Khazraj are with the Department of Energy Technology, Aalborg University, Denmark. e-mail: (mhg@et.aau.dk, clb@et.aau.dk, ffs@et.aau.dk, hkh@et.aau.dk).

H.R. Mohammadi is with Department of Electrical and Computer Engineering, University of Kashan, Iran. e-mail: (mohammadi@kashanu.ac.ir).

H. R. Karami is with the Department of Electrical Engineering, Bu-Ali Sina University, Hamadan, Iran. e-mail: (hamidr.karami@basu.ac.ir).

Paper submitted to the International Conference on Power Systems Transients (IPST2019) in Perpignan, France June 17-20, 2019.

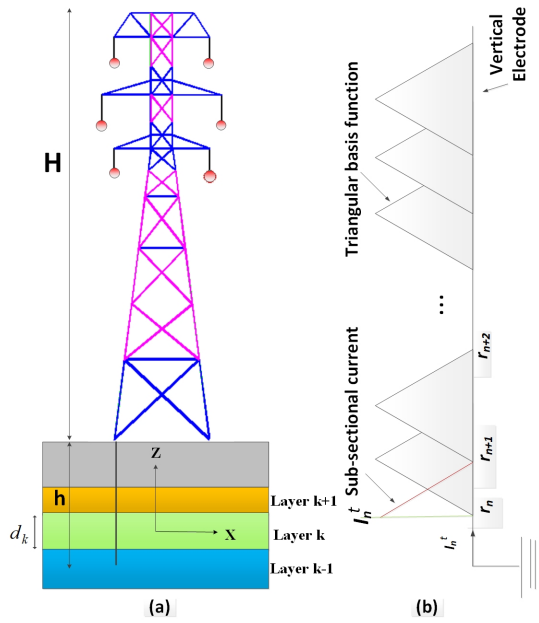


Fig. 1. (a) 2-D model of vertical electrode buried in multilayer soil. (b) triangular basis function of impressed current.

## II. METHODOLOGY

The MoM is used to solve the electrical field integral equation (EFIE), which calculates the distribution of current along vertical electrode for obtaining the input impedance of tower-footing grounding system. Using [16], the current distribution along conductor of grounding system and electric field within the solution domain is calculated by solving the EFIE equation. Eventually, this paper use current and voltage values in impedance matrix form in each frequency. As indicated in Fig. 1(a), the geometry of an idealized multilayer soil (2-D) model was shown. In Fig. 1(b), the impressed-current excitation basis function for input impedance calculation of GS was determined. The electrode is separated into several small segments and the thin wire approximation has used. The governing electric field integral comparison is formulated for determined the current along the grounding conductor segment. The electromagnetic model is employed to achieve spectral domain Green's function, which is classified into and scalar potential  $\Phi$  and magnetic vector potential  $A$ . The spatial domain Green's function is calculated by (1)

$$G^{A,qe} = \frac{1}{2\pi} \int_0^{+\infty} dk_\rho k_\rho J_0(k_\rho \rho) \tilde{G}^{A,qe} \quad (1)$$

where the radial distance in the cylindrical coordinate system is  $\rho$ , Then  $J_0$  and  $k_\rho$  are the zero order Bessel's function and the  $\rho$ -component of the wave vector for the  $G^{th}$  layer, respectively.  $\tilde{G}^{A,qe}$  and  $G^{A,qe}$  indicate spectral domain Green's function and the spatial domain, respectively. Superscripts  $qe$  and  $A$  illustrate the scalar potential and the magnetic vector potential.

Equation (2) shows the magnetic vector potential, the dyadic spatial domain Green's function for magnetic vector potential

is  $\tilde{G}^A$ . The spatial domain Green's function for scalar potential is  $G^{qe}$  [18].

$$\begin{aligned} A(r) &= \int_S \tilde{G}^A(r|r') \cdot I(r') dS' \\ \phi(r) &= \int_S G^{qe}(r|r') \rho_s(r') dS' \end{aligned} \quad (2)$$

The mixed potential integral equation (MPIE) is achieved by employment of boundary condition as (3),

$$\hat{n} \times (E^s(r) + E^{inc}(r)) = 0, \quad r \text{ on } S \quad (3)$$

where  $E^s$  and  $E^{inc}$  stand for the scattered and incident fields respectively. The scattered electric field is explained as (4),

$$E^s(r) = -[j\omega A(r) + \nabla\phi(r)] \quad (4)$$

where  $\omega$ , is angular frequency. The electric current density  $I(r)$  and the electric charge density  $\rho_s(r)$  are presented as (5),

$$\nabla \cdot I(r) = -j\omega\rho_s(r) \quad (5)$$

in the MoM equations, current distribution on the conductor is expanded in finite as (6),

$$I(r) = \sum_{n=1}^N I_n f_n(r) \quad (6)$$

where  $f_n(r)$  and  $I_n$  are the spatial basis function and the unknown current coefficient.  $I_n$  can be find from the resultant matrix equations like follow (7)

$$[A][X] = [B] \quad (7)$$

where  $[A]$ ,  $[X]$ , and  $[B]$  presents the impedance matrix, the unknown vector, and the excitation vector in the MoM.

## III. INPUT IMPEDANCE FOR VERTICAL ELECTRODE BURIED IN MULTILAYER SOIL

To evaluate the effects of electrode length and layers of soil, several GSs contains a single vertical grounding electrode with various lengths and layers analyzed. The maximum length of each meshing element has to be smaller than  $\lambda/10$  where  $\lambda$  is wavelength. The MoM is used for mesh the grounding electrode. The 1 ampere current is injected into the GS at each frequency level and the input impedance  $Z(j\omega)$  of the GS is calculated as a function of frequency. Similarly  $Z(j\omega)$  can be calculated from (7).

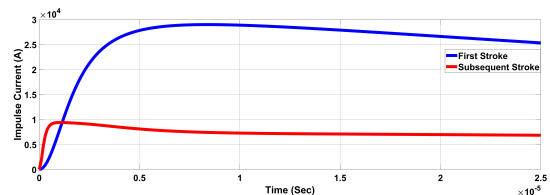


Fig. 2. Waveforms of lightning First and Subsequent return stroke currents adapted from [19].

It is understood that the current distribution depends on the geometry of the GS and the electromagnetic properties of the

soil [8]. The time-domain GPR is acquired as a response to a  $i(t)$  by

$$v(t) = F^{-1}\{Z(j\omega) \cdot F\{i(t)\}\} \quad (8)$$

where  $Z(j\omega)$  presents the input impedance,  $i(t)$  is lightning current, and  $v(t)$  is the GPR at the injection point. In (8),  $F$  and  $F^{-1}$  represents Fourier and inverse fast Fourier transforms (IFFT) [20].

As for the excitation current, the typical waveforms associated with the first and subsequent return strokes are considered, which are described by very high frequency content.

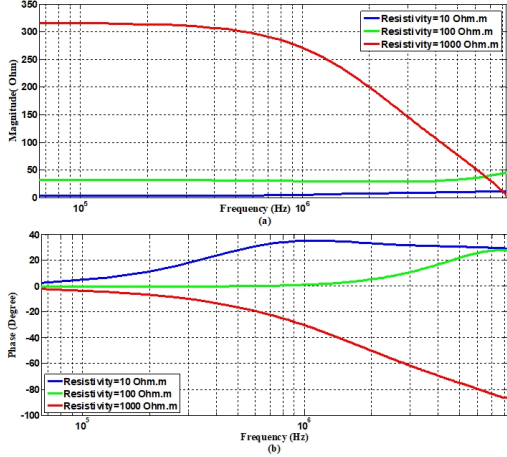


Fig. 3. Input impedance [magnitude (a) and phase (b)] of the vertical electrode buried in homogenous soil with length  $L = 3$ -m. The electrical parameters of soil are characterized by  $\rho = 10, 100$  and,  $1000 \Omega.m$  and  $\epsilon_r = 10$ .

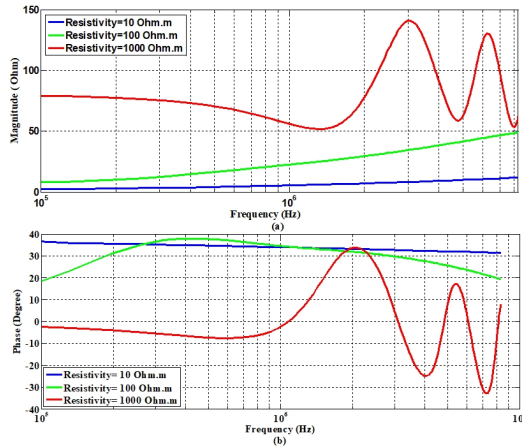


Fig. 4. Input impedance [magnitude (a) and phase (b)] of the vertical electrode buried in homogenous soil with length  $L = 15$ -m. The electrical parameters of soil are characterized by  $\rho = 10, 100$  and,  $1000 \Omega.m$  and  $\epsilon_r = 10$ .

#### A. Adopted Waveforms of Lightning Currents

An authentic assessment of lightning effects on GSs, as well as overvoltages analysis needs a realistic simulation of the lightning current on the tower. Typical waveforms associated with first and subsequent return strokes, which are obtained from Heidler's function [19], are used. Fig. 2 shows the wave

shapes correlated with the lightning first and subsequent return stroke currents, received using Heidler's functions with the parameters presented in Table I. The first stroke waveform simulated by one function and the subsequent stroke by sum of two Heidler's function with the parameters given in Table I [19]. The first return stroke current has peak value of  $30 \text{ kA}$ , zero-to-peak time of  $8 \mu\text{s}$  and maximum steepness of  $12 \text{ kA}/\mu\text{s}$ , whereas the subsequent return stroke current is characterized by a peak value of  $12 \text{ kA}$ , zero-to-peak time of  $0.8 \mu\text{s}$  and maximum steepness of  $40 \text{ kA}/\mu\text{s}$ . Equation (9) presents formula to calculate first and subsequent stroke. It is clear that due to larger rate of rise of the front, subsequent stroke has higher frequency content of in comparison with the first return stroke.

$$i(t) = \frac{I_0}{\eta} \frac{(t/\tau_1)^n}{1+(t/\tau_1)^n} \exp(-t/\tau_2) \quad (9)$$

$$\eta = e^{-\left(\frac{\tau_1}{\tau_2}\right)\left(n\left(\frac{\tau_2}{\tau_1}\right)\right)^{\frac{1}{n}}}$$

where  $\eta$  is amplitude correction factor;  $I_0$  is current pulse

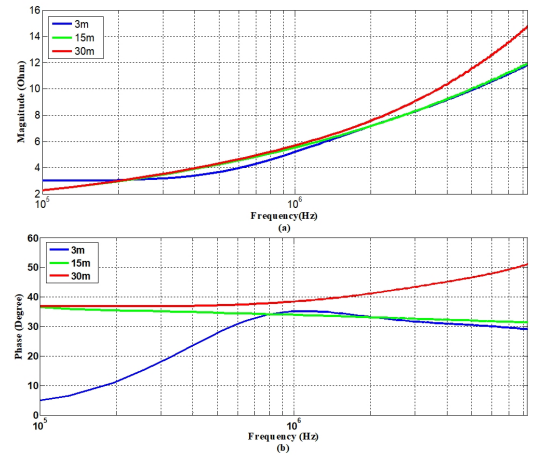


Fig. 5. Input impedance [magnitude (a) and phase (b)] of the vertical electrode lengths of 3-m (blue line), 15-m (green line) and, 30-m (red line) buried in homogenous soil with soil resistivity  $\rho = 10 \Omega.m$  and  $\epsilon_r = 10$

amplitude;  $\tau_1$  front time constant;  $\tau_2$  is delay time constant;  $n$  is exponent having value between 2 to 10.

#### B. Length Electrode Effect on Input Impedance

Assume that the vertical electrode of GS in power transmission line is connected via one-port to one of the tower legs and the cross-section of the vertical rod has a radius of  $12.5\text{-mm}$ . The analysis is presented for several soil resistivity ( $\rho=10, 100, \text{ and } 1000 \Omega.m$ ) with the same relative permittivity of  $\epsilon_r = 10$ . The magnitude of the input impedance in the low frequency range is equal to the static resistance (also called the dc resistance) taking different values for higher frequencies.

Fig. 3 and Fig. 4 show the amplitude and phase of the input impedance for a the vertical electrode of lengths  $L=3$  and  $15$ -m computed using the MoM, respectively. As can be seen in these figures, the input impedance show a frequency-dependent in high frequency range, where input impedance of the tower footing grounding system has a dynamic behavior. Notice also that the behavior of electrode at higher frequencies might be

TABLE I  
HEIDLER'S FUNCTIONS PARAMETERS FOR THE LIGHTNING CURRENTS WAVEFORMS PRODUCING IN FIG. 2 [19].

Parameters	$I_{01}(KA)$	$\tau_{11}(\mu s)$	$\tau_{12}(\mu s)$	$n_1$	$I_{\{02\}}(KA)$	$\tau_{11}(\mu s)$	$\tau_{12}(\mu s)$	$n_2$
First stroke	28	1.8	95	2	-	-	-	-
Subsequent stroke	10.7	0.25	2.5	2	6.5	2.1	230	2

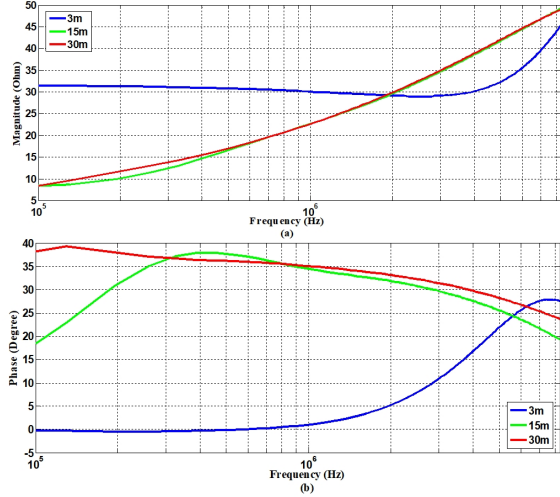


Fig. 6. Input impedance [magnitude (a) and phase (b)] of the vertical electrode lengths of 3-m (blue line), 15-m (green line) and, 30-m (red line) buried in homogenous soil with soil resistivity  $\rho = 100 \Omega.m$  and  $\epsilon_r = 10$ .

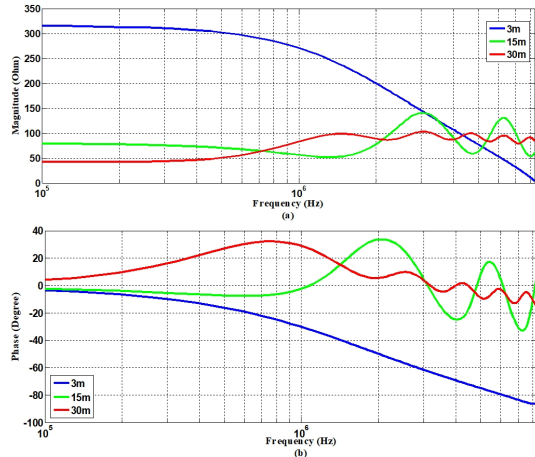


Fig. 7. Input impedance [magnitude (a) and phase (b)] of the vertical electrode lengths of 3-m (blue line), 15-m (green line) and, 30-m (red line) buried in homogenous soil with soil resistivity  $\rho = 1000 \Omega.m$  and  $\epsilon_r = 10$ .

inductive or capacitive. The results shows that the dynamic behavior of electrode depends on length and soil resistivity. In the case of  $L = 3 - m$ ,  $\rho = 1000 \Omega.m$  the electrode behaves as a capacitor and in the of  $L = 15 - m$ ,  $\rho = 1000 \Omega.m$  the electrode behaves as an inductor, whereas that for a lower resistivity of soil ( $\rho = 10 \Omega.m$ ), the behaviour is inductive for both lengths.

Fig. 5, Fig. 6 and 7 show that for soil with high resistivity, the input impedance takes values at high frequencies. Therefore, for high resistivity, GS mostly behaves capacitively, which results in lower impedance. In summary, the input

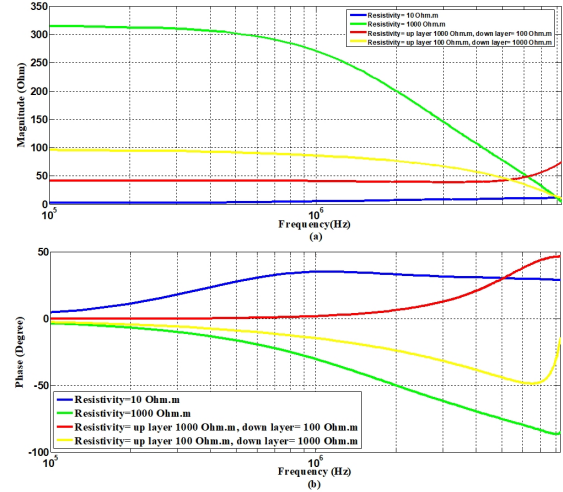


Fig. 8. Input impedance [magnitude (a) and phase (b)] of the vertical electrode with lengths of 3-m buried in homogenous soil and multilayer soil. The soil is characterized by a resistivity of ( $\rho=10 \Omega.m$ ,  $\rho=1000 \Omega.m$ ) for uniform and ( $\rho_1=1000 \Omega.m$ ,  $\rho_2=100 \Omega.m$ ), ( $\rho_1=100 \Omega.m$ ,  $\rho_2=1000 \Omega.m$ ) multilayer soil with a relative permittivity of 10.

impedance might be capacitive or inductive depending on length of electrode and soil resistivity.

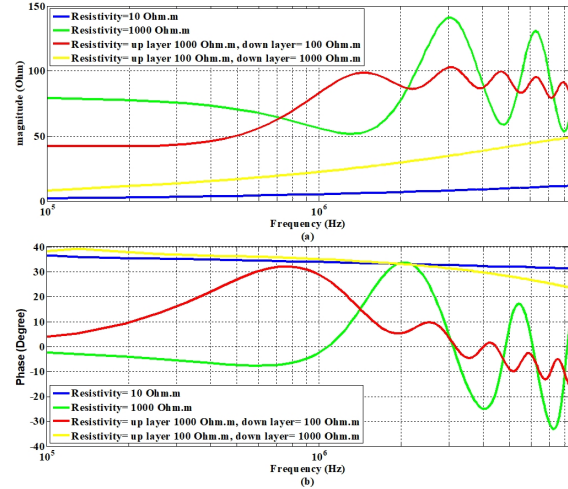


Fig. 9. Input impedance [magnitude (a) and phase (b)] of the vertical electrode with lengths of 15-m buried in homogenous soil and multilayer soil.

### C. Multilayer Effects on Input Impedance of GS

The evaluation of the multilayer soil effects on the input impedance of vertical electrode. This analysis done in the time-domain to obtain GPR, which can be consider as the innovation of the work where other works like [16] did not present it. The length of the electrodes are 3-m, 15-m, and

30-m where buried in a homogenous(uniform) and multilayer soil. The radius of the electrode is 12.5-mm. The depth of the upper soil layer is 1-m. The soil is characterized by a resistivity of ( $\rho=10 \Omega.m$ ,  $\rho=1000 \Omega.m$ ) for uniform and ( $(\rho_1=1000 \Omega.m$ ,  $\rho_2=100 \Omega.m)$ , ( $\rho_1=10 \Omega.m$ ,  $\rho_2=100 \Omega.m$ )) multilayer soil with a relative permittivity of 10. The magnitude and phase

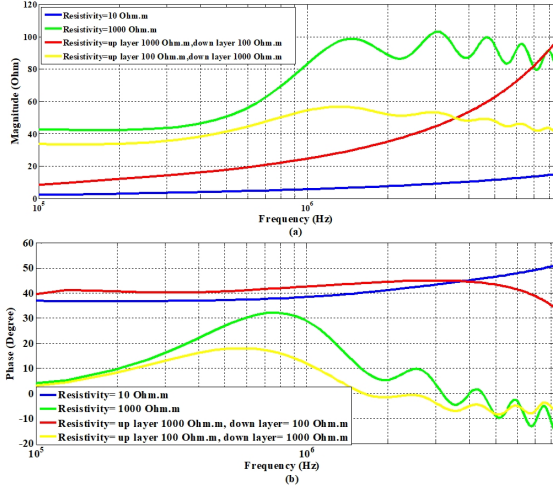


Fig. 10. Input impedance [magnitude (a) and phase (b)] of the vertical electrode with lengths of 30-m buried in homogenous soil and multilayer soil.

impedance for 3-m, 15-m and 30-m vertical electrodes are shown in Fig. 8, 9 and, Fig. 10 respectively. From these figures, it can be seen that the impedance of grounding system and its behavior at high frequency strongly depend on right geometry of electrode and electrical parameters of soil. Fig. 11, Fig.

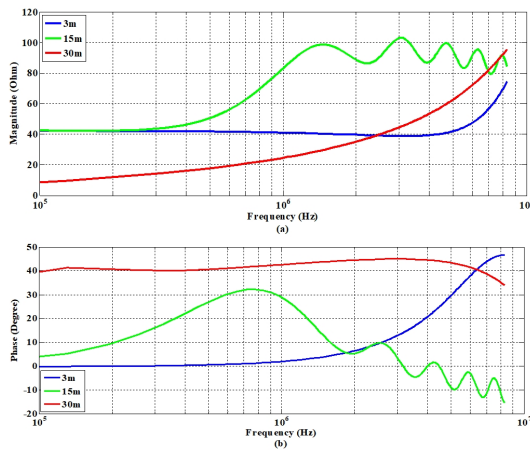


Fig. 11. Input impedance of the vertical electrode with lengths of 3-m, 15-m and, 30-m buried in multilayer soil. magnitude (a) and phase (b) of grounding system with upper layer with soil resistivity of  $\rho_1=1000 \Omega.m$  and lower layer  $\rho_2=100 \Omega.m$ .

12 present the effects of soil resistivity of each layer and length of electrode considering two different multilayer soil with different resistivity. In first case, the resistivity of upper layer is more than lower layer and in the second case, the resistivity of lower layer is more than upper layer. According to the results

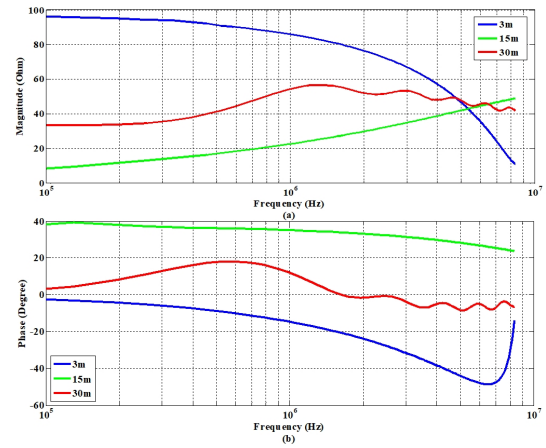


Fig. 12. Input impedance of the vertical electrode with lengths of 3-m, 15-m and, 30-m buried in multilayer soil. magnitude (a) and phase (b) of grounding system with upper layer with soil resistivity of  $\rho_1=100 \Omega.m$  and lower layer  $\rho_2=1000 \Omega.m$ .

when the resistivity of upper layer is more than lower layer, the electrode behaves as an inductor and the magnitude of input impedance will be increase at high frequencies.

#### IV. MULTILAYER EFFECTS AND LENGTH OF VERTICAL ELECTRODE ON GPR

Fig. 13 and Fig. 14 show the GPR computed, considering two type soil (homogenous and multilayer) with three different electrode lengths, 3-m, 15-m and 30-m. The GPRs show large for different length of electrode and electrical parameter of soil show large difference values due to dynamic behavior of electrodes at high frequencies. Therefore, knowing the exact model of GS impacts the estimation of back-flashover and voltage of body tower when the lightning strikes spatially subsequent stroke to power transmission lines. The input impedance of GS were analyzed for multilayer soil with diffrent resistivity and structure. It was obtained that the soil layers have a remarkable contribution in the determination of the input impedance of GS and GPR.

#### V. CONCLUSIONS

The results of a frequency domain of vertical electrode buried in homogenous (uniform), multilayer soil with various geometry and different soil resistivity are briefly described. The subsequent stroke in simulations is used due to the important effects of lightning current high frequency content. A full-wave MoM based on Maxwell's equations are used for evaluation of input impedance of GS. By using input impedance of GS, GPR on power transmission lines is obtained for multilayer soil in time- domain . In final set of results, the effects of wide-band modeling on input impedance on GPR was discussed.

- Discharge time of fast fronted lightning current through the ground depend on inductive or capacitive behavior of electrodes and relates to the fast transient period that lasts few microseconds. After that, the performance of GS is very similar to low frequency resistance (DC resistance).

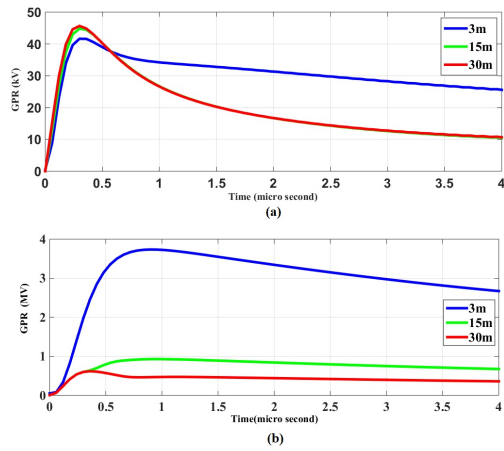


Fig. 13. GPR of a vertical grounding electrode of lengths  $l = 3\text{-m}$ ,  $15\text{-m}$  and,  $30\text{-m}$  and circular cross section of radius  $r = 12.5\text{-mm}$ , buried in a homogenous characterized by a resistivity (a)  $\rho = 10 \Omega.m$ . (b)  $\rho = 1000 \Omega.m$ . and relative permittivity  $\epsilon_r = 10$  subjected to a lightning subsequent return stroke current.

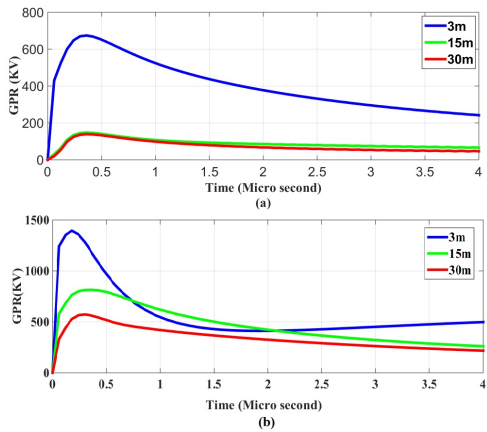


Fig. 14. GPR of a vertical grounding electrode of lengths  $l = 3\text{-m}$ ,  $15\text{-m}$  and,  $30\text{-m}$  and circular cross section of radius  $r = 12.5\text{-mm}$ , buried in multilayer soil characterized by a resistivity (a) ( $\rho_1 = 1000 \Omega.m$ ,  $\rho_2 = 100 \Omega.m$ ) and (b) ( $\rho_1 = 100 \Omega.m$ ,  $\rho_2 = 1000 \Omega.m$ ) and relative permittivity  $\epsilon_r = 10$  subjected to a lightning subsequent return stroke current.

- Taking into account exact model of GS results can be used in no conservative estimate of back-flashover estimation rate.
- It was shown that soil resistivity, electrode length and, layer of soil are the three parameters with higher impact on GPR.

## REFERENCES

- [1] A. R. Hileman, *Insulation coordination for power systems*. CRC Press, 1999.
- [2] IEEE, *IEEE guide for safety in AC substation grounding*. IEEE, 2000.
- [3] B. Shakerighadi, E. Ebrahimzadeh, F. Blaabjerg, and C. L. Bak, "Large-signal stability modeling for the grid-connected VSC based on the lyapunov method," *Energies*, vol. 11, no. 10, p. 2533, sep 2018.
- [4] R. Shariatinasab, J. G. Safar, and H. Falaghi, "Optimisation of arrester location in risk assessment in distribution network," *IET Generation, Transmission & Distribution*, vol. 8, no. 1, pp. 151–159, 2014.

- [5] M. Akbari, K. Sheshyekani, and M. R. Alemi, "The effect of frequency dependence of soil electrical parameters on the lightning performance of grounding systems," *IEEE Transactions on Electromagnetic Compatibility*, vol. 55, no. 4, pp. 739–746, 2013.
- [6] K. Sheshyekani, S. H. H. Sadeghi, R. Moini, F. Rachidi, and M. Paolone, "Analysis of transmission lines with arrester termination, considering the frequency-dependence of grounding systems," *IEEE Transactions on Electromagnetic Compatibility*, vol. 51, no. 4, pp. 986–994, 2009.
- [7] Y. Liu, N. Theethayi, and R. Thottappillil, "An engineering model for transient analysis of grounding system under lightning strikes: Nonuniform transmission-line approach," *IEEE Transactions on Power Delivery*, vol. 20, no. 2, pp. 722–730, 2005.
- [8] L. Qi, X. Cui, Z. Zhao, and H. Li, "Grounding performance analysis of the substation grounding grids by finite element method in frequency domain," *IEEE Transactions on Magnetics*, vol. 43, no. 4, pp. 1181–1184, 2007.
- [9] L. Grcev and M. Popov, "On high-frequency circuit equivalents of a vertical ground rod," *IEEE Transactions on power delivery*, vol. 20, no. 2, pp. 1598–1603, 2005.
- [10] B. Zhang, J. He, J.-B. Lee, X. Cui, Z. Zhao, J. Zou, and S.-H. Chang, "Numerical analysis of transient performance of grounding systems considering soil ionization by coupling moment method with circuit theory," *IEEE Transactions on Magnetics*, vol. 41, no. 5, pp. 1440–1443, 2005.
- [11] Y. Baba, N. Nagaoka, and A. Ametani, "Modeling of thin wires in a lossy medium for fdtd simulations," *IEEE Transactions on Electromagnetic Compatibility*, vol. 47, no. 1, pp. 54–60, 2005.
- [12] A. Otero, J. Cidras, and J. Del Alamo, "Frequency-dependent grounding system calculation by means of a conventional nodal analysis technique," *IEEE Transactions on power delivery*, vol. 14, no. 3, pp. 873–878, 1999.
- [13] K. Sheshyekani, M. Akbari, B. Tabei, and R. Kazemi, "Wideband modeling of large grounding systems to interface with electromagnetic transient solvers," *IEEE Transactions on Power Delivery*, vol. 29, no. 4, pp. 1868–1876, 2014.
- [14] D. Roubertou, J. Fontaine, J. P. Plumey, and A. Zeddou, "Harmonic input impedance of earth connections," in *1984 International Symposium on Electromagnetic Compatibility*, Oct 1984, pp. 1–4.
- [15] L. Grcev, "Modeling of grounding electrodes under lightning currents," *IEEE Transactions on Electromagnetic Compatibility*, vol. 51, no. 3, pp. 559–571, Aug 2009.
- [16] H. Karami, K. Sheshyekani, and F. Rachidi, "Mixed-potential integral equation for full-wave modeling of grounding systems buried in a lossy multilayer stratified ground," *IEEE Transactions on Electromagnetic Compatibility*, vol. 59, no. 5, pp. 1505–1513, 2017.
- [17] B. Honarbakhsh, H. Karami, and K. Sheshyekani, "Direct characterization of grounding system wide-band input impedance," *IEEE Transactions on Electromagnetic Compatibility*, vol. 60, no. 1, pp. 292–293, 2018.
- [18] H. Karami and K. Sheshyekani, "Harmonic impedance of grounding electrodes buried in a horizontally stratified multilayer ground: A full-wave approach," *IEEE Transactions on Electromagnetic Compatibility*, vol. 60, no. 4, pp. 899–906, Aug 2018.
- [19] H. Heidler, "Analytische blitzstromfunktion zur lemp-berechnung," *18th ICLP, Munich, Germany, 1985*, 1985.
- [20] M. Ashouri, F. Faria da Silva, and C. Leth Bak, "Application of short-time fourier transform for harmonic-based protection of meshed vsc-mtdc grids," *The Journal of Engineering*, 2018. [Online]. Available: <https://digital-library.theiet.org/content/journals/10.1049/joe.2018.8765>